Universal Wrinkling of Supported Elastic Rings

Benjamin Foster,[1,*] Nicolás Verschueren,[1,2,†] Edgar Knobloch,[1,‡] and Leonardo Gordillo[3,§]
[1]*Department of Physics, University of California at Berkeley, Berkeley, California 94720, USA*
[2]*College of Engineering, Mathematics and Physical Sciences, University of Exeter, Exeter, EX4 4QF, United Kingdom*
[3]*Departamento de Física, Facultad de Ciencia, Universidad de Santiago de Chile, Estación Central 9170124, Chile*

(Received 14 June 2022; accepted 19 September 2022; published 11 October 2022)

An exactly solvable family of models describing the wrinkling of substrate-supported inextensible elastic rings under compression is identified. The resulting wrinkle profiles are shown to be related to the buckled states of an unsupported ring and are therefore universal. Closed analytical expressions for the resulting universal shapes are provided, including the one-to-one relations between the pressure and tension at which these emerge. The analytical predictions agree with numerical continuation results to within numerical accuracy, for a large range of parameter values, up to the point of self-contact.

DOI: 10.1103/PhysRevLett.129.164301

In-plane buckling of inextensible elastic rings under pressure has been studied over many years [1–4] and exact expressions for the buckled profiles are known [5–7]. Recent interest has centered on the effects of a supporting substrate. The inclusion of substrate forces leads to the emergence of an intrinsic scale λ. When compressed, a substrate-supported ring wrinkles with a critical wavelength defined by this scale instead of simply buckling [8–13]. Periodic buckled and wrinkled states may emerge quasistatically, for example, in externally confined rings [14,15] or crumpled spherical shells [16], in centrifugally or magnetically driven interfacial fingering in a Hele-Shaw cell [17–21], and in the swelling of water-lecithin vesicles [22,23], but may also arise dynamically, for example, during the dynamic collapse of an elastic ring around a soap film [24], the dynamic wrinkling of compressed floating elastica [25], or in pulsating blood vessels [26]. The spatial profiles present in these very different systems are often strikingly similar, and this similarity remains unexplored.

Recent work on a family of simple, yet realistic, models for substrate-supported elastic rings under compression [27] revealed that these models have a special structure that suggests that *exact* wrinkle solutions can be constructed, and that these may, in turn, be related to the well-known buckled states of the substrate-free case. In this Letter, we show that this is indeed the case. Specifically, we show that, for this family of substrate forces, the wrinkle profiles generated by compression are related to the buckled states of the free, unsupported ring [5]. We thereby show that the resulting wrinkle profiles are *universal* for this set of substrate forces. We determine the parameter space mapping that relates the buckled solutions of the classical, unsupported ring problem to the wrinkle solutions for rings with substrate support. We use this mapping to predict bifurcation diagrams for this class of supported-ring problems and test the predictions via numerical continuation.

In order to study the wrinkling of a thin elastic inextensible ring supported by a soft substrate, we consider the following model, which can be derived from the Kirchhoff equations for elastic rods [27,28]:

$$\partial_s^2\kappa + \frac{1}{2}\kappa^3 - T\kappa - P - \frac{1}{2}F(\mathbf{r}) = 0,$$
$$\kappa(s) \equiv \partial_s\phi, \qquad \partial_s\mathbf{r} = (\cos\phi, \sin\phi). \tag{1}$$

As shown in Fig. 1, $\phi(s)$ is the tangential angle relative to the x axis, s is the arclength along the solution profile with length $2\pi R_1$, $\kappa(s)$ is the curvature, and $\mathbf{r}(s) \equiv [x(s), y(s)]$ is the radial vector from the ring center to the point s. The boundary conditions $\phi(2\pi R_1) = \phi(0) + 2\pi$ and the continuity of x, y, $\partial_s\phi$ at $s = 0$ and $2\pi R_1$ rule out nonsmooth solutions. The quantities P and $F(r)$ are the pressure load inward across the ring and the external force per unit of surface due to the substrate, respectively (Fig. 1).

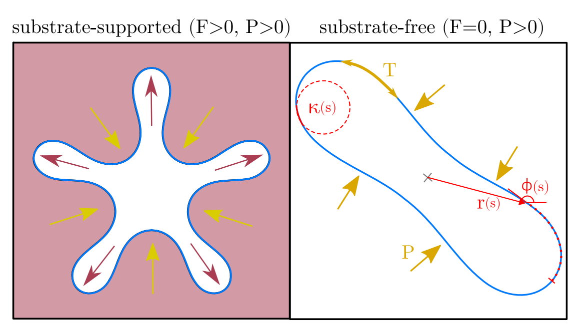

FIG. 1. Possible regimes of interest. The blue curves represent the solution profiles $\mathbf{r}(s)$. Left panel: competition between pressure and substrate forces ($F > 0$) leads to a nontrivial critical wrinkle wave number $m = 5$. Right panel: the substrate-free ($F = 0$) case leads to a buckled state with $m = 2$. The problem variables are shown in the right panel.

The Lagrange multiplier T imposes inextensibility and is a nonlinear eigenvalue related to the tension τ by $T=\tau+\frac{3}{2}\kappa^2$. In particular, we study exact solutions for $F_n(r) = \alpha_n(r^n - r_0^n)$, $n = 0,\ 2,\ 4,\ 6$, where the constant term $\alpha_n r_0^n/2$ is absorbed into P. Our solutions also describe rings tethered to $\mathbf{r} = 0$, provided $F_n(r) = -\alpha_n r^n < 0$ and $P < 0$ (interior overpressure).

The model provides a basis for understanding the nonlinear response of an elastic ring to competing pressure and body forces across a wide range of physical systems. For example, the case $n = 2$ was used as a simple model able to capture the wrinkle-to-smooth transition that takes place in the endothelium of an artery as the internal blood pressure oscillates [27]. In this case, $\alpha_2 = (R_1/\lambda)^5$, where $\lambda \equiv (\mathcal{B}/K)^{1/5}$ is the bending length scale. Here, $\mathcal{B}$ is the bending modulus of the endothelium lining and K is the arterial substrate stiffness. The equations also describe the wrinkling of a circular elastic membrane separating a higher density interior fluid from a lower density exterior fluid in a rotating Hele-Shaw cell [18,19,21]. In this case, $\alpha_2 = \Delta\rho\Omega^2 R_1^5/\mathcal{B}$, where Ω is the rotation rate and $\Delta\rho$ is the density difference between the interior and exterior fluids. In both cases, the wrinkling arises from a competition between the pressure difference favoring buckling and an opposing force generating wrinkling with length scale λ.

Our finding relies on a remarkable feature of weakly nonlinear theory describing periodic perturbations of the circle solution of Eq. (1) in powers of the perturbation amplitude ϵ [27]: for the case $n = 2$, the solution $\phi(s)$ is independent of the force-strength parameter α_2 at every order. To show this we expand ϕ, T, and P in powers of ϵ, and compute the correction terms in $(T, P) = (T_0, P_0) + \epsilon^2(T_2, P_2) + O(\epsilon^4)$ by requiring that the solution at each order is periodic in s with given fundamental wave number m:

$$\phi(s) = s + \epsilon \sin(ms) + \epsilon^2 \frac{\sin(2ms)}{8m} + \mathcal{O}(\epsilon^3). \quad (2)$$

The dependence of P and T on α_2 is linear at every order:

$$T_0 = \frac{1}{2}(1-\alpha_2) - P_0, \quad (3)$$

$$P_2 = \frac{2m^4 - 9m^2 + 3}{8(m^2-1)^2}\alpha_2 + \frac{3(m^2-1)}{8}, \quad (4)$$

$$T_2 = \frac{3}{8(m^2-1)}\alpha_2 + \frac{3(m^2+1)}{8}. \quad (5)$$

Higher order expressions for $\phi_j(s)$ and (T_j, P_j) supporting these observations can be found in the Supplemental Material [29].

The absence of any α_2 dependence in the profile, Eq. (2), has deep physical implications: wrinkle profiles are *universal*, i.e., *identical* wrinkles can be observed on rings with substrates of different strength, or even for the free ring $\alpha_2 = 0$, for appropriate values of the pressure P and tension T. The transformation $(T, P) \to (T, P)$ is linear in α_2 and hence is equivalent to a one-to-one relation between the pressure P and the substrate force measured by α_2. Moreover, since the $\alpha_2 = 0$ problem has closed-form solutions for $\phi(s)$, so does the problem for any $\alpha_2 > 0$. In the following, we demonstrate this fact and determine the transformation $(T,P) \to (T,P)$ that maps a given wrinkle profile at $\alpha_2 > 0$ into the same profile for the free ring $\alpha_2 = 0$.

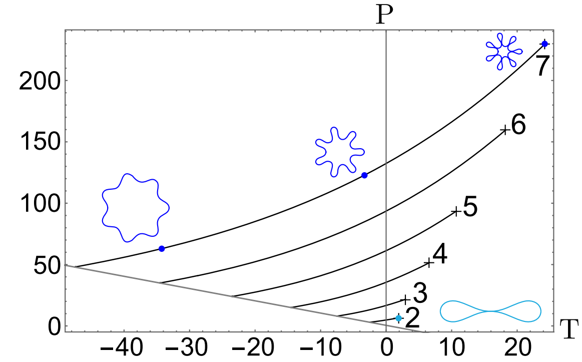

FIG. 2. Free-ring buckling for $F = 0$ and $R_1 = 1$. Solutions with wave numbers $2 \le m \le 7$ (black) bifurcate from the circle solution (gray) as P increases starting with $m = 2$. Sample solution profiles for $m = 2$ (light blue) and $m = 7$ (dark blue) are shown. Crosses represent points of self-contact.

The free inextensible elastic ring problem described by Eq. (1) with $F = 0$ was studied in detail in [2], and is completely integrable [5,30]. Closed-form analytical solutions are known and allow the construction of branches of highly nonlinear wrinkle solutions up to the point of self-contact as shown in the $(T,\ P)$ plane in Fig. 2. The wave numbers m come in in the order $m = 2, 3, \ldots$ as P increases above zero, a consequence of the absence of an intrinsic length scale.

In order to establish the connection between the cases $F = 0$ and $F(r) = \alpha_2 r^2$, we consider the equation for $F = 0$ on a domain of length $2\pi R_2$. This extra degree of freedom is needed to ensure the solutions of both systems are periodic. We define the curvature Q as a function of arclength t and the tension and pressure parameters μ, σ such that

$$\frac{d^2Q(t)}{dt^2} + \frac{1}{2}Q^3(t) - \frac{\mu}{2}Q(t) - \frac{\sigma}{2} = 0. \quad (6)$$

This equation has the integral

$$\left(\frac{dQ}{dt}\right)^2 = 2E - \frac{1}{4}Q^4 + \frac{\mu}{2}Q^2 + \sigma Q, \quad (7)$$

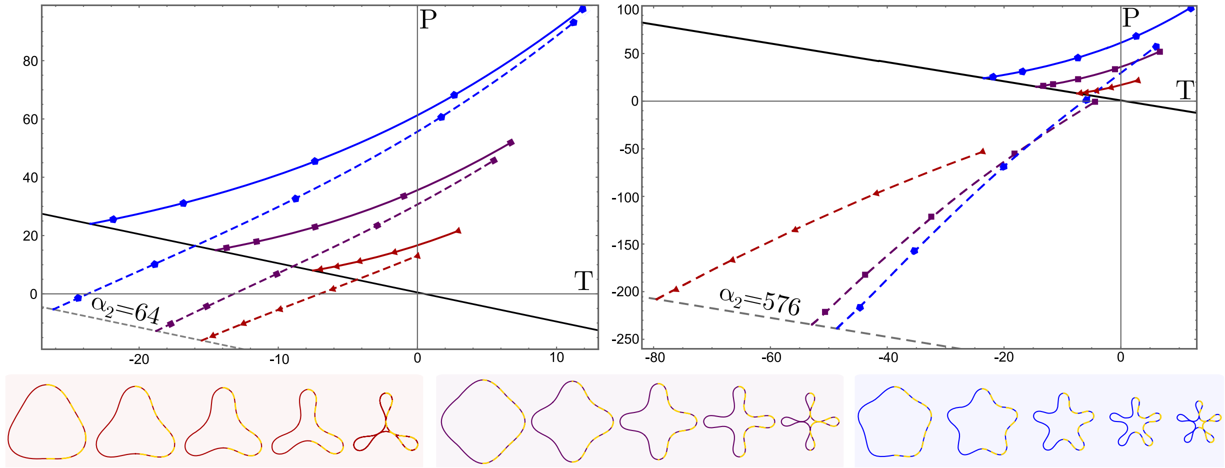

FIG. 3. Top: Numerical continuation for two values of α_2 showing solution branches in the (T, P) plane for $R_1 = 1, R_2 = 3.4108$ and wave numbers $m = 3$ (red triangles), $m = 4$ (purple squares), and $m = 5$ (blue pentagons). Solid lines: $\alpha_2 = 0$ (see Fig. 2); dashed lines $\alpha_2 = 64$ (left) and $\alpha_2 = 576$ (right). Colored markers on the dashed lines map to the corresponding markers on the solid lines. Bottom: Color-coded solution profiles at points indicated in the top panels. The solid profiles show the analytical solution while the superposed orange dashed profiles are from numerical continuation (right half of each profile). The solutions agree to within numerical accuracy. In each case, the final profile corresponds to self-contact.

where E is a constant of integration. We also note a key geometric identity satisfied by the corresponding radius $\rho \equiv \sqrt{X^2 + Y^2}$,

$$\rho^2(t) - \frac{8E + \mu^2}{\sigma^2} - \frac{4Q(t)}{\sigma} = 0, \tag{8}$$

identified in [5]. Equation (6) has exact solutions given by [30]

$$Q(t) = \frac{(A\beta + B\alpha) - (A\beta - B\alpha)\mathrm{cn}(ut, k)}{(A + B) - (A - B)\mathrm{cn}(ut, k)}, \tag{9}$$

where A, B, u, and k are functions of the four roots $\alpha < \beta \in \mathbb{R}$, $\gamma = \bar{\delta} \in \mathbb{C}$ of the quartic polynomial on the right side of Eq. (7), and $\mathrm{cn}(ut, k)$ is the elliptic cosine function with modulus $\sqrt{k}$ (explicit expressions are given in the Supplemental Material [29]). Other solutions exist but are unphysical owing to self-intersection.

Finding an exact physical solution to Eq. (6) then reduces to finding combinations of the three parameters μ, σ, and E that yield closed, non-self-intersecting curves when employed in Eq. (9). Moreover, adding an appropriate multiple of Eq. (8) to Eq. (6) and rescaling $t = sR$, $Q = \kappa/R$, $\rho = rR$, where $R = R_2/R_1$, we obtain

$$\frac{d^2\kappa(s)}{ds^2} + \frac{1}{2}\kappa^3(s) - R^2\left(\frac{\mu}{2} - \alpha_2 \frac{2}{\sigma R^5}\right)\kappa(s) - R^3\left(\frac{\sigma}{2} - \alpha_2 \frac{8E + \mu^2}{2\sigma^2 R^5}\right) - \frac{1}{2}\alpha_2 r^2(s) = 0. \tag{10}$$

There is thus a one-to-one correspondence between Eqs. (1) and (6) under the mapping

$$T = \frac{\mu R^2}{2} - \frac{2\alpha_2}{\sigma R^3}, \tag{11a}$$

$$P = \frac{\sigma R^3}{2} - \frac{8E + \mu^2}{2\sigma^2 R^2}\alpha_2, \tag{11b}$$

$$r^2(s) = \frac{8E + \mu^2}{\sigma^2 R^2} + \frac{4\kappa(s)}{\sigma R^3}. \tag{11c}$$

Consequently, the closed-form analytical solutions of Eq. (6) also apply to Eq. (1) with $n = 2$ and hence describe the wrinkling of rings subject to any force of the form $F \propto r^2$, cf. [7]. The α_2-independent terms in Eqs. (11a), (11b) correspond to the substrate-free tension and pressure. The remaining terms correspond to the additional tension and pressure needed to counteract the substrate force to produce an equivalent spatial profile. The dependence of T and P on both σ, μ, and α_2 leads to a reordering of the branches in the (T, P) plane.

We confirm the analytical results for $\alpha_2 > 0$ obtained with the use of the above mapping using numerical continuation of Eq. (1) in AUTO [31] to show that these correspond to the analytical result [Eq. (9)] at appropriate locations in the (T, P) plane. To do so we solve Eq. (11) using numerically generated values of x, y, κ at known (T, P) to obtain the values of μ, σ, E needed to construct the corresponding solution, Eq. (9). We then use the mapping in Eqs. (11a), (11b) to compare the parameter-space location of these solutions with that of the free-ring problem or to map the free-ring solutions to the corresponding location in parameter space for the substrate-supported ring problem with nonzero α_2. The results for $n = 2$ and two values of α_2 are shown in Fig. 3 for comparison with Fig. 2 and demonstrate perfect agreement

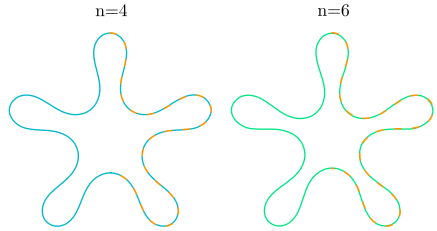

FIG. 4. Analytical solutions ($n = 4$ blue, $n = 6$ green) overlaid with numerical solutions (orange) for $\alpha_{4,6} = 500$ and $R_1 = 1, R_2 = 1$.

between numerical continuation and the closed-form solutions of the free-ring problem at the corresponding points in the (T, P) plane. A quantitative comparison (see Supplemental Material [29]) confirms this geometric universality.

Remarkably, this universality extends beyond $F \propto r^2$: an analogous procedure, involving the addition of powers of the identity Eq. (8) to Eq. (6), can be used to map the free-ring solutions onto a broader family of substrate forces including those for which $n = 4$, 6. A simple translation and rescaling of the curvature (see Supplemental Material [29]) then shows that the free-ring solutions may be used to construct new analytical solutions for both $n = 4$ and $n = 6$. Figure 4 shows overlays of the resulting analytical and numerical solutions for these values of n.

The presence of an additive constant in the curvature results in spatial solutions that are no longer exactly identical, although in the limit of large R or m or small α_n, the additive term is heavily suppressed and the solutions approach a universal profile. In Fig. 5 we show how the geometrical features for $n = 2, 4, 6$ compare across a wide range of α_n and m. The above construction also suggests a straightforward extension to substrate forces of the form $F \sim \sum \alpha_n r^n$, albeit with a more complicated $(T, P) \to (T, P)$ mapping,

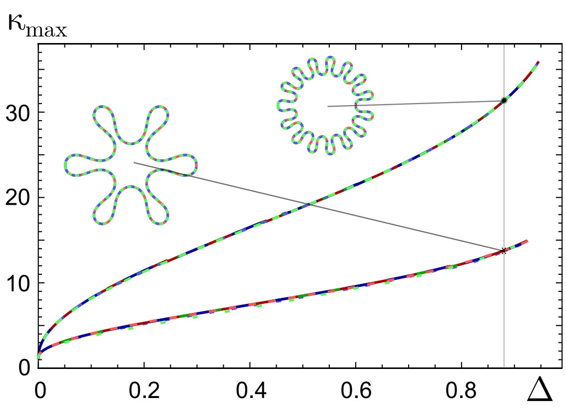

FIG. 5. The compression $\Delta \equiv 1 - A/\pi$ for area A plotted against maximal curvature κ_{max} for $m = 6$ and $m = 15$. Solutions for $n = 2$ (dark red, $\alpha_2 = 10$; light red, $\alpha_2 = 1000$), $n = 4$ (dark blue, $\alpha_4 = 10$; light blue, $\alpha_4 = 1000$), and $n = 6$ (dark green, $\alpha_6 = 10$; light green, $\alpha_6 = 1000$). Solutions are shown at $A = 0.4$ ($\Delta \approx 0.87$) and $R_1 = 1$.

allowing analytical solution of the wrinkle problem with more complex (and more realistic) substrate forces.

Although the wrinkle profiles are the same, the (T, P) mapping modifies the physical response of the system under study as the pressure load increases. In the free-ring problem ($F = 0$) the wave numbers m set in monotonically for $P > 0$ as P increases so the first mode to bifurcate from the circle branch is the $m = 2$ (buckling) mode. As a consequence of the absence of an intrinsic length scale, none of the primary branches ($m = 2, 3, \ldots$) undergoes any secondary bifurcations right up to self-contact. However, when this length scale is present ($\alpha_n > 0$) wrinkle branches may set in in a different order, and the first mode to bifurcate as P increases may have $m > 2$ (wrinkle mode) and set in at negative P. Moreover, as α_n increases, secondary bifurcations move down along the wrinkle branches, eventually passing the point of self-contact. Thus, for large enough α_n, secondary bifurcations take place prior to self-contact, and these generate "folds" if the resulting secondary branch does not connect to another wrinkle branch or "mixed modes" if it does. The mixed modes are characterized by the simultaneous presence of two distinct wave numbers m_1, m_2 whenever they connect primary branches with wave numbers m_1 and m_2 [27]. When $n = 4$, 6, similar structures are observed. Figure 6 shows examples of fold states with intrusion and extrusion, but these are no longer universal and have no counterpart in the free-ring problem with $F = 0$. Mixed states are also present when $n = 4$, 6 but their behavior is complicated by the presence of tertiary bifurcations (not shown). Note that despite the mapping of the wrinkle solutions of Eq. (1) with $\alpha_n > 0$ onto the free-ring problem, the presence of folds (and mixed modes) does require substrate support.

We have shown that equations of the form Eq. (1) possess *identical* closed-form solutions when $n = 0$, 2, albeit at different locations in parameter space, and *near-identical* closed-form solutions when $n = 4$, 6. This is despite the presence of an intrinsic length scale when $\alpha_n > 0$. This remarkable result for $n = 0$, 2 is consistent with the perturbation theory result that ϕ is independent of α_2 to all orders (see Supplemental Material [29]), while T, P do depend on α_2 but only linearly [cf. Eqs. (4) and (5)].

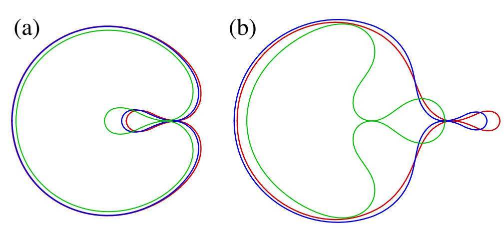

FIG. 6. Secondary fold states for $\alpha_n = 576$ and $R_1 = 1$ at the point of self-contact bifurcating from the first primary branch in each case: $n = 2$ (red, bifurcates from $m = 5$), $n = 4$ (blue, bifurcates from $m = 6$), and $n = 6$ (green, bifurcates from $m = 7$). (a) Fold states with intrusion. (b) Fold states with extrusion. The profiles are strongly dependent on the exponent n.

These facts suggest that we may differentiate Eq. (1) with respect to α_2, yielding

$$T_{\alpha_2}\kappa + P_{\alpha_2} + \frac{1}{2}r^2 = 0, \qquad (12)$$

where T_{α_2}, P_{α_2} are *constants*, an equation that is equivalent to Eq. (11c). Thus, the mapping of Eq. (1) onto the free-ring problem applies to the primary wrinkle solutions for which ϕ is independent of α_2 but not to secondary states where this condition no longer holds. The supported ring problem, Eq. (1), is therefore integrable in this limited sense.

We have presented a simple but tractable mechanics-based model that provides a unified description of the competition between wrinkling and buckling of elastic rings across a family of models characterized by different nonlinear substrate forces. The model predicts the critical pressure for the onset of wrinkling in terms of the mechanical properties of the ring and predicts secondary bifurcations that limit the wrinkling process and initiate folding. Furthermore, the model allowed us to relate the primary wrinkle states to the buckled states of the substrate-free case. Our results are relevant to many fluid-structure interaction problems in both fluid dynamics and biophysics.

This work was supported in part by the National Science Foundation under Grant No. DMS-1908891 (B. F., N. V., and E. K.). The work of N. V. was funded by the National Agency for Research and Development (ANID) through the Scholarship Program: Becas de Postdoctorado en el Extranjero, Becas Chile 2018 No. 74190030. L. G. was funded by Grant ANID/CONICYT FONDECYT Regular 1221103.

[*]Corresponding author.
ben_foster@berkeley.edu
[†]Corresponding author.
nverschueren@berkeley.edu
[‡]Corresponding author.
knobloch@berkeley.edu
[§]Corresponding author.
leonardo.gordillo@usach.cl

[1] M. Lévy, J. Math. Pures Appl. **10**, 5 (1884).
[2] I. Tadjbakhsh and F. Odeh, J. Math. Anal. Appl. **18**, 59 (1967).
[3] J. E. Flaherty, J. B. Keller, and S. I. Rubinow, SIAM J. Appl. Math. **23**, 446 (1972).
[4] J. E. Flaherty and J. B. Keller, SIAM J. Appl. Math. **24**, 215 (1973).
[5] G. Arreaga, R. Capovilla, C. Chryssomalakos, and J. Guven, Phys. Rev. E **65**, 031801 (2002).
[6] P. A. Djondjorov, V. M. Vassilev, and I. M. Mladenov, Int. J. Mech. Sci. **53**, 355 (2011).
[7] P. Djondjorov, V. Vassilev, M. Hadzhilazova, and I. Mladenov, *Proceedings of the Thirteenth International Conference on Geometry, Integrability and Quantization* (Avangard Prima, Sofia, 2012), pp. 107–114.
[8] H. Diamant and T. A. Witten, Phys. Rev. Lett. **107**, 164302 (2011).
[9] L. Pocivavsek, R. Dellsy, A. Kern, S. Johnson, B. Lin, K. Y. C. Lee, and E. Cerda, Science **320**, 912 (2008).
[10] F. Brau, P. Damman, H. Diamant, and T. A. Witten, Soft Matter **9**, 8177 (2013).
[11] M. Rivetti, C. R. Mécanique **341**, 333 (2013).
[12] G. R. Marple, P. K. Purohit, and S. Veerapaneni, Phys. Rev. E **92**, 012405 (2015).
[13] L. Gordillo and E. Knobloch, Phys. Rev. E **99**, 043001 (2019).
[14] A. L. Hazel and T. Mullin, Phil. Trans. R. Soc. A **375**, 20160227 (2017).
[15] G. Napoli and A. Goriely, Proc. R. Soc. A **473**, 20170340 (2017).
[16] G. A. Vliegenthart and G. Gompper, New J. Phys. **13** (2011).
[17] G. D. Carvalho, J. A. Miranda, and H. Gadêlha, Phys. Rev. E **88**, 053006 (2013).
[18] G. D. Carvalho, H. Gadêlha, and J. A. Miranda, Phys. Rev. E **89**, 053019 (2014).
[19] G. D. Carvalho, H. Gadêlha, and J. A. Miranda, Phys. Rev. E **90**, 063009 (2014).
[20] P. O. S. Livera and J. A. Miranda, Phys. Rev. Fluids **5**, 014006 (2020).
[21] L. Carrillo, F. X. Magdaleno, J. Casademunt, and J. Ortín, Phys. Rev. E **54**, 6260 (1996).
[22] W. Harbich, H. Deuling, and W. Helfrich, J. Phys. **38**, 727 (1977).
[23] W. Harbich and W. Helfrich, Chem. Phys. Lipids **36**, 39 (1984).
[24] F. Box, O. Kodio, D. O'Kiely, V. Cantelli, A. Goriely, and D. Vella, Phys. Rev. Lett. **124**, 198003 (2020).
[25] F. Box, D. O'Kiely, O. Kodio, M. Inizan, A. A. Castrejón-Pita, and D. Vella, Proc. Natl. Acad. Sci. U.S.A. **116**, 20875 (2019).
[26] S. K. Veerapaneni, R. Raj, G. Biros, and P. K. Purohit, Int. J. Nonlinear Mech. **44**, 257 (2009).
[27] B. Foster, N. Verschueren, E. Knobloch, and L. Gordillo, New J. Phys. **24**, 013026 (2022).
[28] B. Audoly and Y. Pomeau, *Elasticity and Geometry* (Oxford University Press, New York, 2010).
[29] See Supplemental Material at http://link.aps.org/supplemental/10.1103/PhysRevLett.129.164301 for supporting analytical and numerical computations.
[30] V. M. Vassilev, P. A. Djondjorov, and I. M. Mladenov, J. Phys. A **41**, 435201 (2008).
[31] E. J. Doedel, A. R. Champneys, T. Fairgrieve, Y. Kuznetsov, B. Oldeman, R. Paffenroth, B. Sandstede, X. Wang, and C. Zhang, AUTO-07P: Continuation and Bifurcation Software for Ordinary Differential Equations (Concordia University, Montreal, 2012).